APL Materials

Defect-induced magnetism in homoepitaxial $SrTiO_3$

Cite as: APL Mater. **10**, 091108 (2022); https://doi.org/10.1063/5.0101411
Submitted: 31 May 2022 • Accepted: 23 August 2022 • Published Online: 20 September 2022

A. D. Rata, J. Herrero-Martin, I. V. Maznichenko, et al.

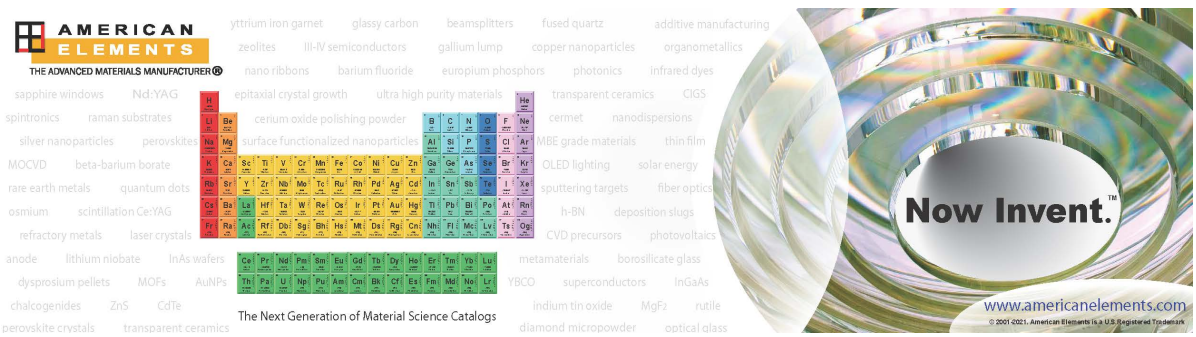

AIP Publishing

Defect-induced magnetism in homoepitaxial $SrTiO_3$

Cite as: APL Mater. 10, 091108 (2022); doi: 10.1063/5.0101411
Submitted: 31 May 2022 • Accepted: 23 August 2022 •
Published Online: 20 September 2022

View Online Export Citation CrossMark

A. D. Rata,[1] J. Herrero-Martin,[2] I. V. Maznichenko,[1] F. M. Chiabrera,[3] R. T. Dahm,[3] S. Ostanin,[1] D. Lee,[4] B. Jalan,[4] P. Buczek,[5] I. Mertig,[1] A. Ernst,[6,7] A. M. Ionescu,[8] K. Dörr,[1] N. Pryds,[3,a)] and D.-S. Park[8,a)]

AFFILIATIONS

[1] Institut für Physik, Martin-Luther-Universität Halle-Wittenberg, 06120 Halle, Germany
[2] ALBA Synchrotron Light Source, Cerdanyola del Vallès, 08290 Barcelona, Spain
[3] Department of Energy Conversion and Storage, Technical University of Denmark, DK-2800 Kgs Lyngby, Denmark
[4] Department of Chemical Engineering and Materials Science, University of Minnesota-Twin Cities, Minneapolis, Minnesota 55455, USA
[5] Department of Engineering and Computer Sciences, Hamburg University of Applied Sciences, 20099 Hamburg, Germany
[6] Max-Planck-Institut für Mikrostrukturphysik, 06120 Halle, Germany
[7] Institute of Theoretical Physics, Johannes Kepler University, 4040 Linz, Austria
[8] Laboratory for Nanoelectronic Devices, Swiss Federal Institute of Technology-EPFL, 1015 Lausanne, Switzerland

Note: This paper is part of the Special Topic on Materials Challenges and Synthesis Science of Emerging Quantum Materials.
[a)]**Authors to whom correspondence should be addressed:** nipr@dtu.dk and dspark1980@gmail.com

ABSTRACT

Along with recent advancements in thin-film technologies, the engineering of complex transition metal oxide heterostructures offers the possibility of creating novel and tunable multifunctionalities. A representative complex oxide is the perovskite strontium titanate (STO), whose bulk form is nominally a centrosymmetric paraelectric band insulator. By tuning the electron doping, chemical stoichiometry, strain, and charge defects of STO, it is possible to control the electrical, magnetic, and thermal properties of such structures. Here, we demonstrate tunable magnetism in atomically engineered STO thin films grown on STO (001) substrates by controlling the atomic charge defects of titanium (V_{Ti}) and oxygen (V_O) vacancies. Our results show that the magnetism can be tuned by altering the growth conditions. We provide deep insights into its association to the following defect types: (i) V_{Ti}, resulting in a charge rearrangement and local spin polarization, (ii) V_O, leading to weak magnetization, and (iii) V_{Ti}–V_O pairs, which lead to the appearance of a sizable magnetic signal. Our results suggest that controlling charged defects is critical for inducing a net magnetization in STO films. This work provides a crucial step for designing magnetic STO films via defect engineering for magnetic and spin-based electronic applications.

INTRODUCTION

Strontium titanate (SrTiO3, STO) has a cubic ABO_3 perovskite structure (space group: *Pm*-3*m*, a lattice constant of a = 3.905 Å) at room temperature (RT). It is a nonmagnetic band insulator with an indirect bandgap of 3.25 eV separating the valence band O 2*p* states and the lowest unoccupied Ti 3*d* t_{2g} states of the conduction band.[1,2] STO has a large dielectric constant of about 300 at room temperature in a low electric field and exhibits a quantum paraelectric behavior at very low temperatures, i.e., a suppression (in the ~20–100 K range) of the ferroelectric transition by quantum fluctuations.[2,3] The electrically insulating phases of STO can be made conductive (i) by replacing oxygen atoms with oxygen vacancies, which then act as donor-type dopants or (ii) by subtle chemical doping, e.g., Nb (0.1%)-doped STO. Both undoped and Nb-doped STO single crystals have been widely used as substrates for the growth of oxide films. STO-based structures have shown a rich diversity of remarkable properties including low-temperature high (~10^4 $cm^2V^{-1}s^{-1}$) electron mobility,[4–6] superconductivity below 300–500 mK,[7,8] room-temperature ferroelectricity,[9,10] large

dielectric constants (ε_r = ~10^3 at RT),[9,11] room-temperature ferromagnetism,[12] and nonvolatile resistive switching.[13] These interesting properties of STO can be obtained through delicate control of the electron doping (via chemical dopants such as La or Nb), variations in the stoichiometry, strain-induced symmetry breaking, and defect engineering. As a result of this panoply of material properties, for more than half a century, engineered perovskite STO materials and STO-based homo-/heterostructures have attracted considerable scientific interest and become integral materials for oxide-based electronic device applications.

In particular, inducing magnetism in STO thin films can be accomplished through modifications to the lattice strain by employing lattice-mismatched single crystalline oxide substrates (e.g., biaxial strain = −1.16% and +1.29% for $NdGaO_3$ and $TbScO_3$, respectively) and/or by controlling cation stoichiometry (Sr or Ti deficiency) and oxygen vacancy (V_O) concentrations.[14–18] Defects typically result in lattice expansion and a charge rearrangement in STO. This can lead to lattice symmetry breaking (electric polarization), followed by an electronic reconstruction and crystal field splitting (e.g., splitting of degenerate Ti $3d_{t_{2g},e_g}$ orbitals into a relative energy scheme that follows $d_{xz}/d_{yz} < d_{xy} < d_{3z^2-r^2} < d_{x^2-y^2}$).[19,20] The origin of magnetism in STO has remained a long-standing problem, and the presence of V_O defects has been widely regarded as one of the main contributors to magnetization: Oxygen vacancies allow the partial reduction of Ti^{4+} into magnetically active Ti^{3+}. A few examples of some of the proposed mechanisms are listed here: Coey *et al.* suggested that the origin of ferromagnetism in reduced STO is either due to direct exchange interactions between V_O and the molecular orbitals of valence electrons of surrounding Ti ions or due to a Stoner-type spin-splitting of the Ti 3*d* band for ferromagnetically coupled electrons.[12] However, Brovko and Tosatti[21] reported theoretical results suggesting that an isolated V_O defect in STO only stabilizes states with low or zero total magnetization since the two Ti spins facing each other across the V_O are antiferromagnetically coupled via strong direct exchange interaction. Doenning and Pentcheva[22] demonstrated that in $LaAlO_3$ (LAO)/STO heterostructures, Ti d_{xy} bands could be dominantly magnetized via magnetic double-exchange interactions between Ti^{3+} and Ti^{4+} when a tensile in-plane strain is induced in TiO_6 octahedra and the electron doping level is below 7 × 10^{14} cm^{-2}. However, this electron doping level (0.5e per Ti) per STO monolayer is hard to achieve practically when considering that Ti d_{xy} orbital polarization in a *c*-axis compressed STO is purely induced by a high V_O concentration of ~25 at. % as a V_O sublattice. Note that it was found that the perovskite lattice of $SrTiO_{3-x}$ retains a V_O concentration of ≤5.6 at. %.[23] Similar V_O-mediated Ti magnetization levels have been observed experimentally in reduced STO ceramics,[12,24] STO thin films,[25] STO-based heterostructures (e.g., LAO/STO interfaces),[26] and reduced TiO_{2-x}.[27] However, these examples show very weak magnetic responses, which do not appear robust enough to be employed practically. Importantly, it was also found that in the absence of V_O defects, magnetism can still occur in these systems by controlling cation off-stoichiometry (e.g. Ti vacancies).[28–30] The above observations indicate that magnetism in the STO system might be induced by contributions of both cation and anion defects. Hence, understanding the role of these defects is of critical importance for creating and controlling the associated magnetism in STO.

In this work, we demonstrate tunable magnetic properties of homoepitaxial STO thin films by controlling both cation off-stoichiometry (V_{Ti}) and V_O contents using pulsed laser deposition (PLD). Our results show that oxygen partial pressure (P_O) strongly influences the growth dynamics and the magnetization of the films. We found incorporating both V_{Ti} and V_O defects into the lattice structure can enhance magnetism up to a threshold concentration at which a strong charge compensation occurs. We have used first-principles calculations to classify the effects of individual defects and complex defect pairs on the development of a magnetic response in STO, conclusions which are supported by x-ray magnetic circular dichroism (XMCD) measurements. Our results show that manipulating the oppositely charged atomic defects in STO is the key to creating and tuning magnetism in STO thin films.

RESULTS AND DISCUSSION

Epitaxial STO films were grown on TiO_2-terminated STO(001) substrates [Fig. 1(a)] using a pulsed laser deposition (PLD) system equipped with reflection high-energy electron diffraction (RHEED), which was used to control the thickness of the deposited films. The substrate temperature was kept at 700 °C and a laser repetition rate of 1 Hz was employed for the film growth. The laser-beam spot size on the STO target was ~4.5 mm^2. To obtain the growth of B-site cation deficient STO films, we employed a consistent low laser fluence (e.g., ~0.6 J/cm^2) during film growth, based on our previous work.[29] Meanwhile, the background oxygen partial pressure was varied from P_O = 5 × 10^{-2} mbar to 5 × 10^{-6} mbar. In addition, in order to examine the effect of V_O concentration on the magnetism of the films, we used different cooling processes after film growth: (i) in a high oxygen atmosphere (200 mbar O_2) or (ii) in the same atmosphere that was used during film growth.

In PLD, laser fluence strongly influences the kinetic energy of the ablated species, which, in turn, affects the adatom mobility at the substrate surface, thereby also affecting the ablation rate and film thickness.[31] Especially, when considering the growth of complex compound materials, an inadequate fluence can preferentially ablate certain elements over others, which results in the formation of cation nonstoichiometric films.[29–33] It should be noted that preferential ablation happens above a threshold ablation rate. Due to its impact on the ablation rates of various elements, laser fluence has been used in literature to control the stoichiometry of STO films:[29,32,33] In the case of STO, a preferential ablation of Ti (Sr) can be induced by increasing (decreasing) laser fluence, leading to the formation of Sr-(Ti-) deficient STO films. Since the kinetic energy of the arriving species is affected also by the background pressure in the chamber, P_O, during the PLD process, a suitable balance between the laser fluence and background gas is essential.[31,34] Thus, controlling the relation between the laser fluence and P_O is an effective way to induce and control atomic defects in the films.

Figure 1(b) shows RHEED intensity oscillations for STO film growth at different P_O: 5 × 10^{-2} mbar, 5 × 10^{-4} mbar, and 5 × 10^{-6} mbar. The overall thickness of the films was kept around 25–26 nm. The appearance of persistent RHEED oscillations indicates that the growth of STO films occurred in layer-by-layer growth mode. However, it was found that the RHEED intensity dampened faster when P_O was decreased. P_O influences the growth rate (pulses

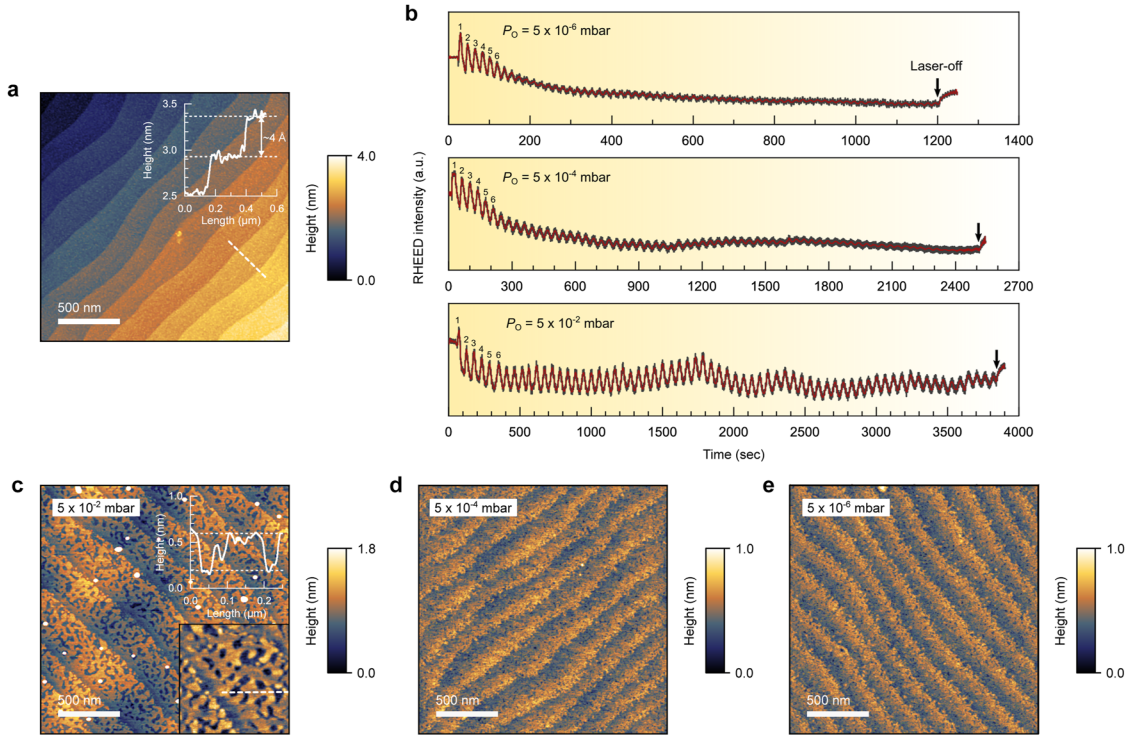

FIG. 1. (a) A topography AFM image (3 × 3 μm^2) of atomically terminated TiO_2-terminated STO(001) substrate, used for this work. (b) RHEED intensity oscillations for the layer-by-layer STO film growth with different P_O. [(c)–(e)] Topography AFM images (3 × 3 μm^2) for the grown films in P_O = 5 × 10^{-2} mbar (c), 5 × 10^{-4} mbar (d), and 5 × 10^{-6} mbar (e). The insets in (c) show a height profile for an incomplete STO monolayer at the step-terrace surface.

needed per unit cell, pls/uc) of the films, which for our experiments was found to be ~57 pls/uc at 5 × 10^{-2} mbar, ~37 pls/uc at 5 × 10^{-4} mbar, and ~18 pls/uc at 5 × 10^{-6} mbar. This P_O-dependent growth rate variation can be attributed to the change of plasma plume dynamics during film growth, i.e., the higher the P_O, the more confined the plume expansion. In addition, the stoichiometric composition was found to scale with background P_O.[34] When the background pressure is high, transport occurs in a diffusion-like regime and Ti and Sr atoms can be fully oxidized in the plasma plume. In contrast, under low background pressures, the interactions between the ablated species and the background gas in the plume are minor and the species in the plume have high kinetic energies and travel following ballistic-like motion. It is particularly in this low pressure regime where preferential elemental ablation can be effectively driven by applying an inadequate laser fluence, thus intentionally controlling the cation off-stoichiometry of STO thin films. This is due to relatively large weight ratios of Ti/Sr (0.56), compared to that of TiO_2/SrO (0.77).[34] At low P_O values, around 5 × 10^{-6} mbar, cation off-stoichiometry is observed in the rapid damping of the RHEED intensity during the STO film growth [Fig. 1(b)]. The film variation as a function of P_O is reflected also in the surface morphology of the grown films as shown in Figs. 1(c)–1(e). For P_O = 5 × 10^{-2}, an atomically flat morphology was found with a terrace step height of ~4 Å [Fig. 1(c)], similar to the vicinal step-structure of the TiO_2-terminated STO surface. Note that the atomic force microscopy (AFM) image [Fig. 1(c)] shows an incomplete STO monolayer at the step-terrace surface—the height difference within the terrace is around 4 Å. In contrast, at $P_O \leq 5 \times 10^{-4}$, the film surface is facetted due to the ballistic motion of the arriving species to the substrates. These results provide a solid indication that the growth dynamics and chemical plasma composition of the STO films can be effectively tuned by P_O, while the laser fluence is kept constant at a low value.

Figure 2(a) shows the high-resolution x-ray diffraction (XRD) 2θ-ω patterns of oxidized STO films, grown on STO(001), as a function of P_O. Note that all of the measured films were cooled down to RT in an O_2 atmosphere (200 mbar). The XRD spectra show that the oxidized films were grown epitaxially and possess thickness fringes. The STO film grown at P_O = 5 × 10^{-2} mbar shows almost identical 2θ (00l) peak positions to those of the STO homo-substrate with well-defined thickness fringes. This indicates low out-of-plane strain (x_z = +0.19%) in the film and an excellent crystal quality. When P_O was decreased to P_O = 5 × 10^{-4} mbar, a continuous shift of the out-of-plane STO(00l) peaks toward lower 2θ values was found. This reveals an increase in the c-axis lattice parameter to a value of c = 3.95 Å (x_z = +1.15%), as shown in Fig. 2(c). To get further information about the strain distribution of the STO films, we performed reciprocal space mappings (RSMs) around the STO103 reflection for the two films (with P_O = 5 × 10^{-2} and 5 × 10^{-4} mbar) [Fig. 2(b)]. The results show that the in-plane lattice spacing for both films is

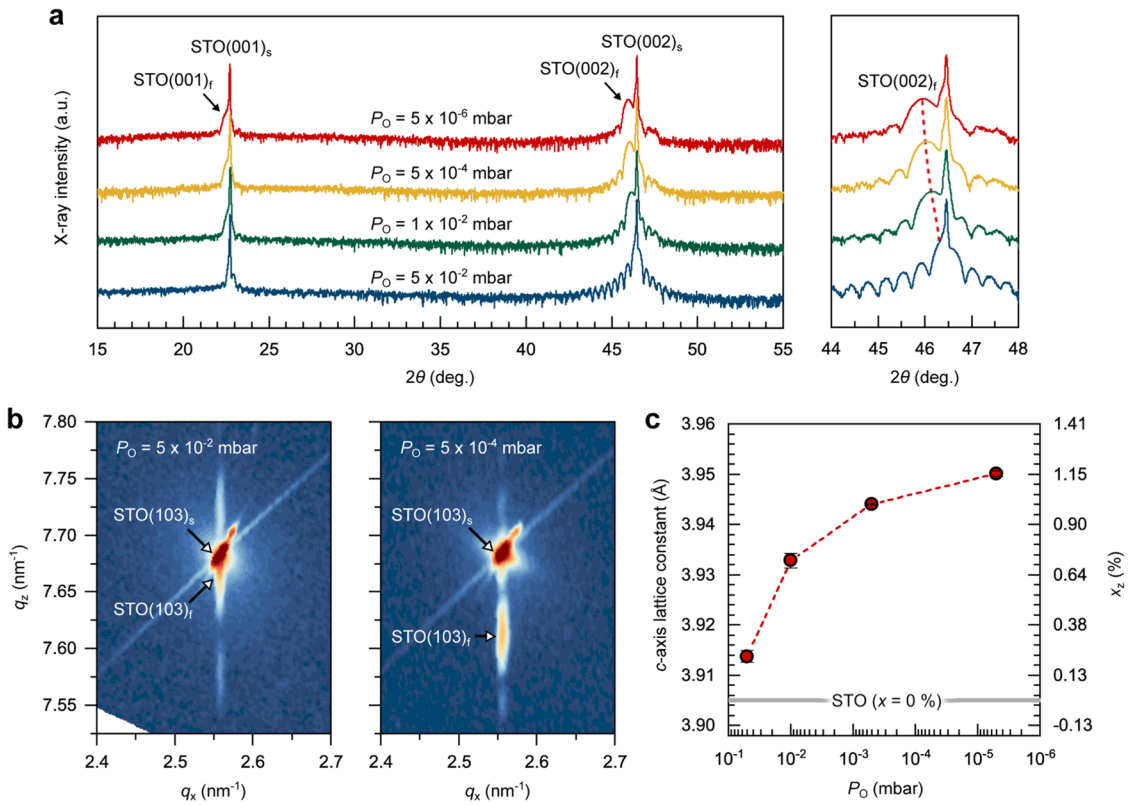

FIG. 2. (a) XRD 2θ scans for the STO films, grown on STO(001) substrates, as a function of P_O. The right panel shows the XRD (002) peaks for the STO films and substrates. (b) RSM near STO103 reflection for the STO films grown at $P_O = 5 \times 10^{-2}$ and 5×10^{-4} mbar. (c) Variations in the *c*-axis lattice parameter (left) and strain (right) of the films with different P_O.

coherently aligned with the in-plane spacing of the underlying STO substrates ($a = 3.905$ Å), while the *c*-axis lattice parameter was found to increase with P_O [Fig. 2(c)].

We investigated the magnetic properties of the oxidized STO films using a superconducting quantum interference device (SQUID) magnetometer. Prior to the sample measurement, external magnetic effects {e.g., sample holders, low-temperature glue, instrumental accessories, and annealed TiO_2-STO substrates [see Fig. 5(a)]} were carefully eliminated.[29] Figure 3(a) shows the in-plane magnetic hysteresis loops of the STO films, measured at 5 K, as a function of P_O. The results show a notable increase in the magnetization with decreasing P_O. The saturation magnetic moment of the films continuously increases up to 14 μemu (56 μemu/cm^2) as the growth pressure is decreased to a value of $P_O = 5 \times 10^{-4}$ mbar. The enhanced magnetism at low P_O can be understood through the rise of cation off-stoichiometry (Ti deficiency) in the films. We can rule out that the increase in magnetization results from external magnetic impurities that may have been present in the target materials or in the PLD growth chamber since our results show the opposite trend from what would be expected if this was the case. Lower P_O values (up to 5×10^{-4} mbar) yield higher film growth rates and, thus, require a shorter total film growth time (decreasing the time that the films are exposed to external impurities) [Fig. 1(b)]; nonetheless, they produce larger magnetic moments. Another important observation is the steep magnetic degradation (≤10 μemu) seen in the STO film grown at $P_O = 5 \times 10^{-6}$ mbar. To confirm this, we repeated the film growth with the same growth conditions and observed the same weak magnetic response as compared to the results obtained using $P_O = 5 \times 10^{-4}$ mbar. We postulate that this magnetic degradation could be associated with a strong charge compensation between positively and negatively charged V_O and V_{Ti} defects as the oxidized film sample, grown at $P_O = 5 \times 10^{-6}$ mbar, shows a pale gray color. Further oxidation (200 mbar O_2 annealing at 500 °C for 2 h) will eventually cause the formation of a secondary phase (see the supplementary material, Fig. S1).

To understand atomic charge defect-mediated magnetism in STO, we performed first-principles calculations on STO with atomic vacancy defects. Density functional theory (DFT) simulations using VASP code[35] were performed to calculate the electronic, structural, and magnetic properties of ABO_3-perovskite STO by incorporating all possible atomic vacancy defects (V_{Ti}, V_{Sr}, and V_O). The structural relaxation simulation was performed using a 4 × 4 × 4 **k**-mesh and the conjugate-gradient algorithm until the Hellmann–Feynman forces became less than 5×10^{-3} eV/Å. The density of states (DOS) was then obtained using the Γ-centered and compacted **k**-mesh with minor smearing of 10 meV. The

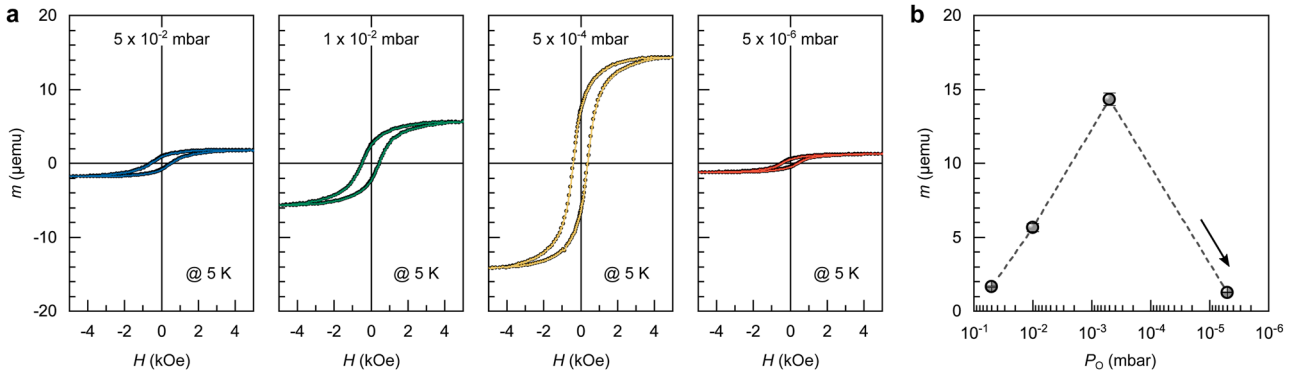

FIG. 3. (a) The 5 K magnetic hysteresis loops of the STO films, grown at different P_O (=5 × 10^{-2}, 1 × 10^{-2}, 5 × 10^{-4}, and 5 × 10^{-6} mbar). (b) Variations in the magnetic moment of the films as a function of P_O.

Perdew–Burke–Ernzerhof (PBE) generalized-gradient approximation (GGA)[36] was applied to the exchange-correlation potential. The use of GGA-PBE and its reliability were discussed previously for simulations of the STO structures. Detailed calculation methods are presented elsewhere.[29,37]

Figure 4(a) illustrates a STO model structure with a Ti vacancy (V_{Ti}) defect (~2 at. %) separated by a regular distance of 4*a* (where *a* is the lattice constant). Together with the atomic rearrangement (which produces a local lattice expansion of ~1.1%) of the six oxygen neighbors surrounding the V_{Ti}, a visible magnetic response in the model structure was found: The O and Ti ions neighboring a V_{Ti} site became spin-polarized through charge rearrangement, yielding a μ_B/V_{Ti} of 0.48. It should be noted that the V_{Ti} site itself has no magnetic moment. The cation vacancy-induced magnetic moments

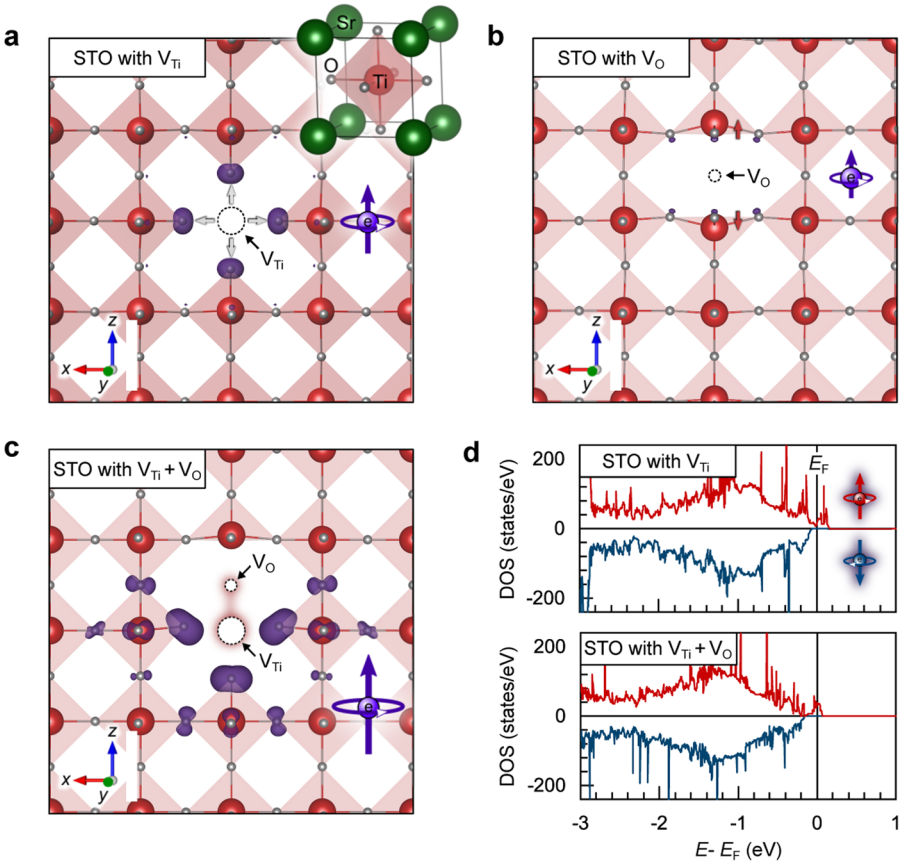

FIG. 4. [(a)–(c)] Magnetization density of the ABO_3-perovksite STO structures, induced by different atomic vacant defects, a V_{Ti} (a), a V_O (b), and a V_{Ti}-V_O pair (c). (d) Spin-polarized density of states of the STO with a V_{Ti} (upper panel) and with a V_{Ti}-V_O pair (lower panel).

show a dome-shaped dispersive magnetic nature over the surrounding lattices, mostly on the nearest oxygen atoms. The calculated spin-polarized density of states (DOS) of the system further indicates that the negatively charged V_{Ti} in STO behaves as a *p*-type like acceptor locally and leads to the effective spin-polarization of the six nearest oxygen atoms due to unsaturated valence electrons, O 2*p* electrons (about 70% of the induced magnetization). In this case, a relatively weak Ti magnetization occurs via spin-polarized charge transfer through a *p*-*d* band hybridization. Furthermore, we considered the effect of A-site Sr (2+) vacancies on the magnetism of STO. An A-site vacancy defect contributes to a relatively weak magnetization of $m < 0.07\ \mu_B/V_{Sr}$ in STO due to its much less effective charge rearrangement:[29] (i) Only two electrons can contribute to the oxygen atoms adjacent to a Sr vacancy site and (ii) a Sr vacant site has a relatively large distance (2.76 Å) to the 12 nearest oxygens as compared to that (1.95 Å) of a Ti vacant site. In a STO model structure with V_O defects (~1 at. %), separated by a 4*a* distance [Fig. 4(b)], the positively charged V_O acts like an *n*-type donor in the system and the local lattice expansion occurs primarily by moving the two neighboring Ti atoms upward. Our calculations show that an isolated V_O when stabilized in STO produces a very weak magnetism ($0.003\ \mu_B/V_O$) without significant exchange interaction with the neighboring Ti atoms (e.g., a magnetization of Ti d_{xy} bands). This is consistent with previous reports.[21] When the Vo concentration increases up to ~8 at. %, the defects are placed in STO with a separating distance of $\sqrt{2}a$ (in an orthorhombic $\sqrt{2} \times \sqrt{2} \times 2$ supercell) and the Ti d_{xy} bands become magnetized with a total moment of $0.41\ \mu_B/V_O$. However, such a defect sublattice in STO with high V_O concentration is highly unrealistic as an artificial magnetic array since it is hard to retain an ABO_3-perovskite structure practically.[17]

Next, we examined a STO model structure incorporating both cation and anion vacancy defects. Our results show that a V_O defect energetically tends to be paired with a V_{Ti} in STO after relaxation [Fig. 4(c)]. The results of the model indicate that the atomic configuration in which the vacancies are 1/2*a* apart is much more energetically favorable than pairing at a distance of 3/2*a* by an energetic difference of ~1 eV. We found that in an unrelaxed model structure, the complex defect pair creates a magnetic spin-moment of $2\ \mu_B$/pair in the system due to an incomplete charge compensation and the relaxation of the oppositely charged V_{Ti} (4+) and V_O (2−) vacancies. After atomic relaxation with charge screening, the system has a total magnetization of $0.7\ \mu_B$/pair. The calculated DOS clearly shows a spin-polarized moment distribution near the Fermi level of the system [Fig. 4(d)]. Interestingly, the magnetization of STO induced by the defect pair is higher than the moments for individual cation defects, despite the fact that the defect charge state of V_{Ti} (4+) is higher than that of V_{Ti}–V_O (2+). Our calculations clarify that the large measured magnetization is produced by the V_{Ti}–V_O pair due to (i) a more energetically stable formation (smaller charge screening effect) in the STO system with a tendency of pairing the oppositely charged defects [when comparing the charge screening effect of STO with a singular V_{Ti} through relaxation and the largely varied magnetization ($4\ \mu_B/V_{Ti} \rightarrow 0.48\ \mu_B/V_{Ti}$)], (ii) a higher dispersive nature of the induced magnetic moment over the lattice atoms, and (iii) an effective magnetic coupling with a shorter distance (3.5*a*) between the vacant defect pairs. However, it should be noted that an excessive concentration of V_O defects in the system can compensate for the charge state of the defect pair. This mechanism could produce a significant degradation in the defect-induced magnetism of STO as can be seen in our experimental results [Fig. 3(b)].

To examine the effect of the V_{Ti}–V_O defect pair on the magnetism of STO, we prepared B-site cation deficient STO films with different V_O concentrations. To achieve this, different cooling processes were applied after film growth, i.e., cooling to room temperature in a high O_2 atmosphere (200 mbar) and under the same P_O as used during growth. Figure 5(a) shows the magnetic hysteresis loops of the STO films measured at 5 K. These two samples were grown using the same laser fluence of ~0.6 J/cm^2 at a pressure of $P_O = 5 \times 10^{-4}$ mbar, using the two cooling procedures described above. Notably, the magnetic moment of the STO film cooled down in the same P_O increases by a factor of ~3.5 when compared to that of the film cooled in O_2 atmosphere. This magnetic enhancement is indicative of an increase in the formation of V_{Ti}–V_O defect pairs in STO driven by the P_O cooling process. Furthermore, to examine magnetic effects of a reduced STO substrate and possible impurities in the PLD chamber, we annealed a TiO_2-terminated STO substrate by using the same heating rate (to 700 °C) and P_O cooling process in the PLD vacuum chamber that was used for film growth. The annealed STO substrate shows no magnetic response [Fig. 5(a)], confirming that the P_O cooling process at 5×10^{-4} mbar (V_O) cannot solely create the observed magnetism of the B-site cation deficient STO films. These results indicate either that the employed P_O does not create a sufficient number of V_O sites for achieving ferromagnetic ordering in STO or that the number of V_O sites plays a minor role in creating the magnetism. Moreover, both B-site cation deficient films show a similar temperature-independent magnetic response in the range of 5–300 K. Such temperature-independent magnetizations for materials with high Curie temperatures of ≫300 K were also attributed to defect-induced magnetism (e.g., ZnO, MgO, TiO_2, and HfO_2).[12,28,30,38] These are most likely explained by a spin-splitting of the defect-related impurity bands near the conduction band/valence band edge of the systems, as these are the source for ferromagnetically coupled electrons.[12] Our experimental results confirm that the magnetism of STO can be controlled by incorporating both V_{Ti} and V_O defects, which probably promotes the formation of V_{Ti}–V_O pairs. However, the replacement of B-site cation with V_O defects in STO should be limited (by using P_O ~5×10^{-4} mbar in our case) in order to obtain such a magnetic enhancement and to prevent a strong atomic charge compensation, e.g., $1V_{Ti}$ (4+) + $2V_O$ (2−).

We further verified the magnetic nature of the B-site cation deficient STO film by x-ray magnetic circular dichroism (XMCD). The Ti $L_{2,3}$-edge x-ray absorption (XAS) spectra were collected by using circular polarized light with parallel (μ_+) and antiparallel (μ_-) photon spin while applying a constant magnetic field of +1 T perpendicular to the sample surface, with the probing depth being around 4 nm. The spectra were collected with the beam in normal incidence. The total electron yield method was used to record the spectra (by measuring the sample drain current) in a chamber with a vacuum base pressure of 2×10^{-10} mbar. Figure 5(c) shows the Ti $L_{2,3}$-edge XAS and XCMD spectra of the B-site cation deficient STO film sample that was cooled down to RT at the

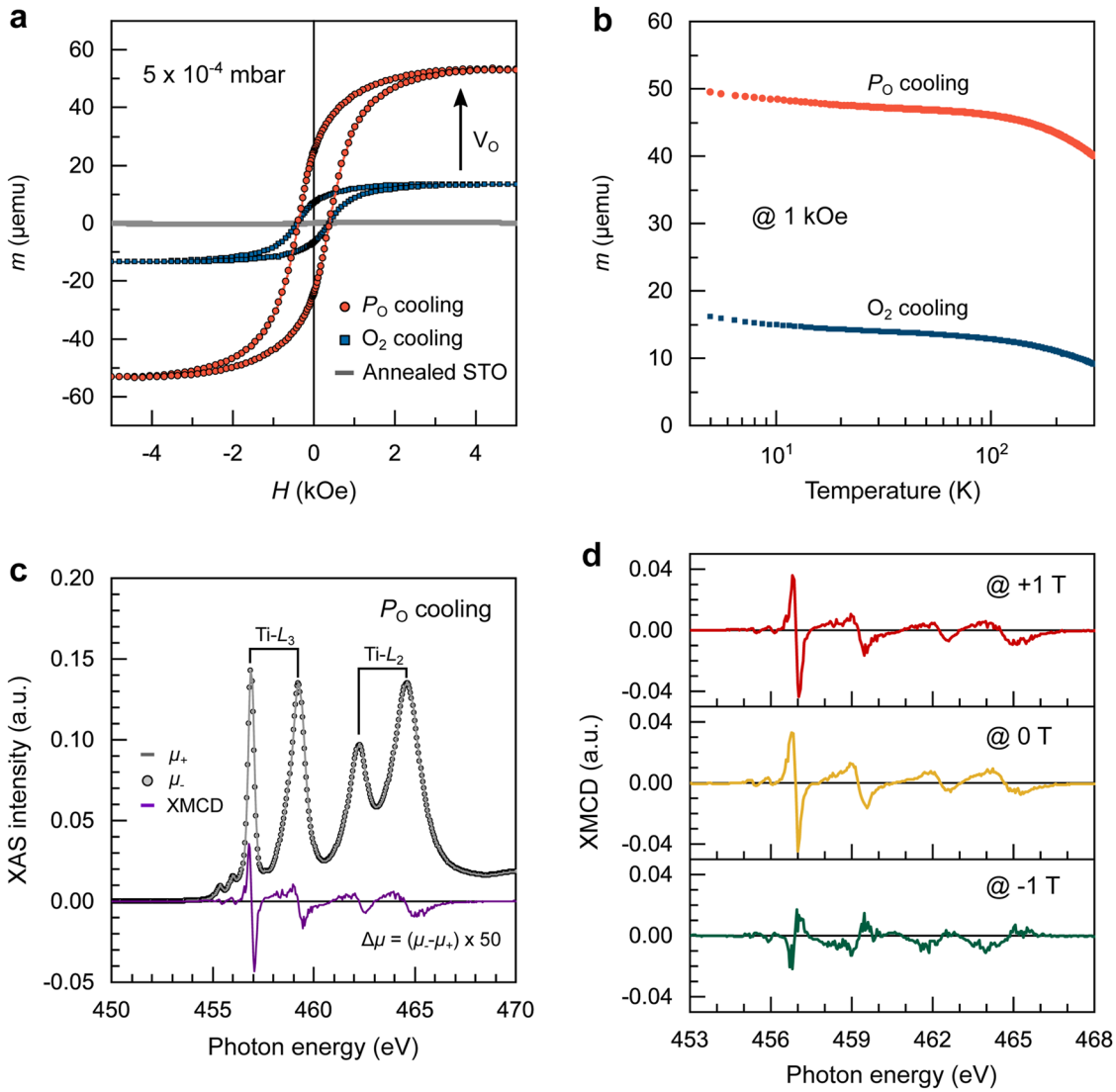

FIG. 5. (a) Comparison of the 5 K magnetic hysteresis loops of the B-site cation deficient STO films, grown at $P_O = 5 \times 10^{-4}$ mbar, with different cooling processes, i.e., after film growth, the two samples were cooled in a high O_2 atmosphere (blue circle, O_2 cooling) and in the same growth pressure (red circle, P_O cooling) separately. The hysteretic magnetic responses of the two STO/STO samples are compared with a non-magnetic annealed TiO_2-STO(001) substrate. (b) Variable temperature magnetic moments of the samples, prepared by different cooling processes. A constant magnetic field of 1 kOe was applied to the samples during the temperature measurements. (c) XAS and XMCD across the Ti $L_{2,3}$-edges of the B-site cation deficient STO film sample with P_O cooling as measured at 4 K. (d) Ti $L_{2,3}$ XMCD of the same STO thin film as measured by sweeping the applied magnetic fields (+1 T → 0 T → −1 T).

same P_O as the deposition pressure. First, we discard the possibility of the magnetic signal being due to the presence of Ti (3+) states since the spectral shape is typical of pure Ti (4+) as reported previously.[39–41] This indicates that the Ti $L_{2,3}$ XMCD signal probably stems from the excitation between the Ti^{4+} $3d^0$ and O $2p$ orbitals: the Ti^{4+} ($3d^0$) ions are related to the magnetic environment sensitivity of the electrons excited to the $2P^5 3d^1$ state. The increased number of defect pairs in the STO film should enhance the magnetization of the surrounding Ti atoms. Furthermore, the reversible XMCD signal under applied field inversion confirms the true magnetic nature of the STO films [see Fig. 5(d)]. As a result, the XMCD analysis suggested that the defect-induced magnetism in the engineered STO films is due to the contribution of p-type like defects that spread magnetic moments over the surrounding ions. The magnetism of the engineered STO films is unlikely to be due to an accumulation of magnetic Ti^{3+} ions or any associated magnetic order.

CONCLUSION

In this work, we have demonstrated that the magnetic properties of engineered STO thin films can be effectively tuned by PLD film growth parameters (interdependent parameters of laser fluence and P_O) by controlling the concentration of cation vacancies, anion vacancies, and their complex defects. Our results show that B-site cation vacancies, V_{Ti}, not only contribute to the magnetization of STO but also promote the incorporation of oppositely charged V_O into the B-site cation deficient STO for the formation of the V_{Ti}–V_O pairs. This greatly increases the magnetization and stability of the system and has been demonstrated both experimentally and theoretically. We further show that a strong charge compensation between oppositely charged defects significantly reduces the magnetism of STO, suggesting that under these process conditions, oxygen vacancies are not the main magnetic source for the defect-mediated magnetism of STO since we have not detected the presence of magnetic Ti^{3+}. Therefore, such a design allowing for tunable magnetism in STO films via atomic defect engineering offers important insights into the possible routes for designing magnetic STO films and related oxide heterosystems.

SUPPLEMENTARY MATERIAL

See the supplementary material for XRD 2θ patterns of the as-grown and O_2-annealed B-site cation deficient STO film samples, grown at 5×10^{-6} mbar (Fig. S1).

ACKNOWLEDGMENTS

D.-S. Park and N. Pryds acknowledge the support provided by the European Commission through the project Biowings H2020 FET-OPEN 2018–2022 (Grant No. 80127). N. Pryds acknowledges funding from Villum Fonden for the NEED project (Grant No. 00027993) and the Danish Council for Independent Research Technology and Production Sciences for the DFF-Research Project 3 (Grant No. 00069 B). D. Lee and B. Jalan acknowledge support from the Air Force Office of Scientific Research (AFOSR) through Grant Nos. FA9550-21-1-0025 and FA9550-21-0460. We thank Thierry Désiré Pomar for reading the manuscript.

AUTHOR DECLARATIONS

Conflict of Interest

The authors have no conflicts to disclose.

Author Contributions

A. D. Rata: Investigation (equal); Writing – review & editing (equal). **I. Mertig**: Investigation (equal); Writing – review & editing (equal). **A. Ernst**: Investigation (equal); Writing – review & editing (equal). **A. M. Ionescu**: Investigation (equal); Writing – review & editing (equal). **K. Dörr**: Investigation (equal); Writing – review & editing (equal). **N. Pryds**: Conceptualization (equal); Funding acquisition (equal); Supervision (equal); Writing – original draft (equal); Writing – review & editing (equal). **D.-S. Park**: Conceptualization (equal); Data curation (equal); Formal analysis (equal); Funding acquisition (equal); Investigation (equal); Methodology (equal); Project administration (equal); Resources (equal); Supervision (equal); Validation (equal); Visualization (equal); Writing – original draft (equal); Writing – review & editing (equal). **J. Herrero-Martin**: Investigation (equal); Writing – review & editing (equal). **I. V. Maznichenko**: Investigation (equal); Writing – review & editing (equal). **F. M. Chiabrera**: Investigation (equal); Writing – review & editing (equal). **R. T. Dahm**: Investigation (equal); Writing – review & editing (equal). **S. Ostanin**: Investigation (equal); Writing – review & editing (equal). **D. Lee**: Investigation (equal); Writing – review & editing (equal). **B. Jalan**: Investigation (equal); Writing – review & editing (equal). **P. Buczek**: Investigation (equal); Writing – review & editing (equal).

DATA AVAILABILITY

The data that support the findings of this study are available within the article.

REFERENCES

[1] A. S. Bhalla, R. Guo, and R. Roy, Mater. Res. Innovations **4**, 3 (2000).
[2] Y.-Y. Pai, A. Tylan-Tyler, P. Irvin, and J. Levy, Rep. Prog. Phys. **81**, 036503 (2018).
[3] R. A. Cowley, Phys. Rev. **134**, A981–A997 (1964).
[4] H. P. R. Frederikse and W. R. Hosler, Phys. Rev. **161**, 822–827 (1967).
[5] J. Son, P. Moetakef, B. Jalan, O. Bierwagen, N. J. Wright, R. Engel-Herbert, and S. Stemmer, Nat. Mater. **9**, 482–484 (2010).
[6] J. Yue, Y. Ayino, T. K. Truttmann, M. N. Gastiasoro, E. Persky, A. Khanukov, D. Lee, L. R. Thoutam, B. Kalisky, R. M. Fernandes, V. S. Pribiag, and B. Jalan, Sci. Adv. **8**, eabl5668 (2022).
[7] J. F. Schooley, W. R. Hosler, and M. L. Cohen, Phys. Rev. Lett. **12**, 474 (1964).
[8] K. Ahadi, L. Galletti, Y. Li, S. Salmani-Rezaie, W. Wu, and S. Stemmer, Sci. Adv. **5**, eaaw0120 (2019).
[9] J. H. Haeni, P. Irvin, W. Chang, R. Uecker, P. Reiche, Y. L. Li, S. Choudhury, W. Tian, M. E. Hawley, B. Craigo, A. K. Tagantsev, X. Q. Pan, S. K. Streiffer, L. Q. Chen, S. W. Kirchoefer, J. Levy, and D. G. Schlom, Nature **430**, 758 (2004).
[10] D. Lee, H. Lu, Y. Gu, S.-Y. Choi, S.-D. Li, S. Ryu, T. R. Paudel, K. Song, E. Mikheev, S. Lee, S. Stemmer, D. A. Tenne, S. H. Oh, E. Y. Tsymbal, X. Wu, L.-Q. Chen, A. Gruverman, and C. B. Eom, Science **349**, 1314 (2015).
[11] M. Lippmaa, N. Nakagawa, M. Kawasaki, S. Ohashi, Y. Inaguma, M. Itoh, and H. Koinuma, Appl. Phys. Lett. **74**, 3543 (1999).
[12] J. M. D. Coey, M. Venkatesan, and P. Stamenov, J. Phys.: Condens. Matter **28**, 485001 (2016).
[13] M. Janousch, G. I. Meijer, U. Staub, B. Delley, S. F. Karg, and B. P. Andreasson, Adv. Mater. **19**, 2232 (2007).
[14] K. T. Kang, H. I. Seo, O. Kwon, K. Lee, J.-S. Bae, M.-W. Chu, S. C. Chae, Y. Kim, and W. S. Choi, Appl. Surf. Sci. **499**, 143930 (2020).
[15] E. Breckenfeld, R. Wilson, J. Karthik, A. R. Damodaran, D. G. Cahill, and L. W. Martin, Chem. Mater. **24**, 331 (2012).
[16] G. Z. Liu, Q. Y. Lei, and X. X. Xi, Appl. Phys. Lett. **100**, 202902 (2012).
[17] A. Ohtomo and H. Y. Hwang, J. Appl. Phys. **102**, 083704 (2007).
[18] H. N. Lee, S. S. A. Seo, W. S. Choi, and C. M. Rouleau, Sci. Rep. **6**, 19941 (2016).
[19] T. Li, S. Deng, H. Liu, S. Sun, H. Li, S. Hu, S. Liu, X. Xing, and J. Chen, Adv. Mater. **33**, 2008316 (2021).
[20] Y. Cao, X. Liu, P. Shafer, S. Middey, D. Meyers, M. Kareev, Z. Zhong, J.-W. Kim, P. J. Ryan, E. Arenholz, and J. Chakhalian, npj Quant. Mater. **1**, 16009 (2016).
[21] O. Brovko and E. Tosatti, Phys. Rev. Mater. **1**, 044405 (2017).
[22] D. Doenning and R. Pentcheva, Sci. Rep. **5**, 7909 (2015).
[23] W. Gong, H. Yun, Y. B. Ning, J. E. Greedan, W. R. Datars, and C. V. Stager, J. Solid State Chem. **90**, 320 (1991).

[24]D. A. Crandles, B. DesRoches, and F. S. Razavi, J. Appl. Phys. **108**, 053908 (2010).
[25]W. Xu, J. Yang, W. Bai, K. Tang, Y. Zhang, and X. Tang, J. Appl. Phys. **114**, 154106 (2013).
[26]M. Salluzzo, S. Gariglio, D. Stornaiuolo, V. Sessi, S. Rusponi, C. Piamonteze, G. M. De Luca, M. Minola, D. Marre', A. Gadaleta, H. Brune, F. Nolting, N. B. Brookes, and G. Ghiringhelli, Phys. Rev. Lett. **111**, 087204 (2013).
[27]S. D. Yoon, Y. Chen, A. Yang, T. L. Goodrich, X. Zuo, D. A. Arena, K. Ziemer, C. Vittoria, and V. G. Harris, J. Phys.: Condens. Matter **18**, L355 (2006).
[28]K. Potzger, J. Osten, A. A. Levin, A. Shalimov, G. Talut, H. Reuther, S. Arpaci, D. Bürger, H. Schmidt, T. Nestler, and D. C. Meyer, J. Magn. Magn. Mater. **323**, 1551 (2011).
[29]D.-S. Park, A. D. Rata, I. V. Maznichenko, Y. Gan, S. Ostanin, S. Agrestini, M. Walker, G. J. Rees, Y. Chen, P. Muralt, I. Mertig, K. Dörr, A. Ernst, and N. Pryds, Nat. Commun. **11**, 3650 (2020).
[30]S. Wang, L. Pan, J.-J. Song, W. Mi, J.-J. Zou, L. Wang, and X. Zhang, J. Am. Chem. Soc. **137**, 2975 (2015).
[31]A. Ojeda-G-P, M. Döbeli, and T. Lippert, Adv. Mater. Interfaces **5**, 1701062 (2018).
[32]T. Ohnishi, M. Lippmaa, T. Yamamoto, S. Meguro, and H. Koinuma, Appl. Phys. Lett. **87**, 241919 (2005).
[33]D. J. Keeble, S. Wicklein, R. Dittmann, L. Ravelli, R. A. Mackie, and W. Egger, Phys. Rev. Lett. **105**, 226102 (2010).
[34]K. Orsel, R. Groenen, B. Bastiaens, G. Koster, G. Rijnders, and K.-J. Boller, APL Mater. **3**, 106103 (2015).
[35]G. Kresse and J. Furthmüller, Phys. Rev. B **54**, 11169 (1996).
[36]J. P. Perdew, K. Burke, and M. Ernzerhof, Phys. Rev. Lett. **77**, 3865 (1996).
[37]I. Maznichenko, S. Ostanin, A. Ernst, and I. Mertig, Phys. Rev. Mater. **3**, 074006 (2019).
[38]P. Esquinazi, W. Hergert, D. Spemann, A. Setzer, and A. Ernst, IEEE Trans. Magn. **49**, 4668 (2013).
[39]J. R. L. Mardegan, D. V. Christensen, Y. Z. Chen, S. Parchenko, S. R. V. Avula, N. Ortiz-Hernandez, M. Decker, C. Piamonteze, N. Pryds, and U. Staub, Phys. Rev. B **99**, 134423 (2019).
[40]J.-S. Lee, Y. W. Xie, H. K. Sato, C. Bell, Y. Hikita, H. Y. Hwang, and C.-C. Kao, Nat. Mater. **12**, 703 (2013).
[41]N. Ortiz Hernández, Z. Salman, T. Prokscha, A. Suter, J. R. L. Mardegan, S. Moser, A. Zakharova, C. Piamonteze, and U. Staub, Phys. Rev. B **103**, 224429 (2021).